

Camera-Based Short Physical Performance Battery and Timed Up and Go Assessment for Older Adults With Cancer

Larry Duncan, *Student Member, IEEE*, Shaotong Zhu, Mackenzi Pergolotti^{ID}, Smith Giri, Hoda Salsabili, Miad Faezipour^{ID}, *Senior Member, IEEE*, Sarah Ostadabbas^{ID}, *Member, IEEE*, and S. Abdollah Mirbozorgi^{ID}, *Member, IEEE*

Abstract—This paper presents an automatic camera-based device to monitor and evaluate the gait speed, standing balance, and 5 times sit-stand (5TSS) tests of the Short Physical Performance Battery (SPPB) and the Timed Up and Go (TUG) test. The proposed design measures and calculates the parameters of the SPPB tests automatically. The SPPB data can be used for physical performance assessment of older patients under cancer treatment. This stand-alone device has a Raspberry Pi (RPi) computer, three cameras, and two DC motors. The left and right cameras are used for gait speed tests. The center camera is used for standing balance, 5TSS, and TUG tests and for angle positioning of the camera platform toward the subject using DC motors by turning the camera left/right and tilting it up/down. The key algorithm for operating the proposed system is developed using Channel and Spatial Reliability Tracking in the cv2 module in Python. Graphical User Interfaces (GUIs) in the RPi are developed to run tests and adjust cameras, controlled remotely via smartphone and its Wi-Fi hotspot. We have tested the implemented camera setup prototype and extracted all SPPB and TUG parameters by conducting several experiments on a human subject population of 8 volunteers (male and female, light and dark complexions) in 69 test runs. The measured data and calculated outputs of the system consist of tests of gait speed (0.041 to 1.92 m/s with average accuracy of >95%), and standing balance, 5TSS, TUG, all with average time accuracy of >97%.

Index Terms—5 times sit-stand, gait speed, image processing, object recognition, short physical performance battery (SPPB), standing balance, Timed Up and Go (TUG).

I. INTRODUCTION

UP TO 60% of all new cancer diagnoses and 70% of all cancer related deaths occur in adults 65 years and above [1]. By 2026 it is expected that over 20 million Americans will be cancer survivors (people living on with a cancer diagnosis) [2]. Many have high symptom burden that reduces their quality of life physically, socially, and cognitively, which may lead to disability [3]. In particular, older adults receiving cancer treatment have an increased risk of functional decline, disability, health care use, and hospitalization [4]. There is a critical need to personalize cancer treatment of older adults by assessing their physical performance and estimating their tolerance of treatment [5]. Performance based measures of physical activity are recommended and can help determine this anticipated tolerability, however they are not currently incorporated in standard clinical practice because of time and resource constraints [6], [7].

As part of physical assessment, the Short Physical Performance Battery (SPPB) is recognized as an objective way to measure lower extremity function. It includes three performance-based measures: walking speed over 4 m at a normal speed, time to perform 5 chair-stands, and 10-second standing balance tests (feet semi-tandem, side-by-side, and tandem) [8]. In clinical practice, the SPPB can be done manually by the clinical team (using stopwatch) with the patient at a clinic. However, because of time and resource constraints, such measurements are not routinely done for older adults with cancer [9]. For older adults with cancer, objective measurement of SPPB by clinical personnel is very important for baseline evaluation measurement, treatment planning, and subsequent progress monitoring during clinic visits. Similar to the SPPB, the Timed Up and Go (TUG) test provides objective data on the quality of mobility and fall risk among older adults with cancer, which can be used clinically to determine tolerability of cancer treatment and need for supportive interventions [10]. To meet this requirement, new automated tools to check physical status are needed to obtain measurement with less clinical personnel support time.

Manuscript received 4 November 2022; revised 20 January 2023 and 17 February 2023; accepted 27 February 2023. Date of publication 6 March 2023; date of current version 30 August 2023. (Corresponding author: S. Abdollah Mirbozorgi.)

Larry Duncan is with the Electrical and Computing Engineering Department, The University of Alabama at Birmingham, USA.

Shaotong Zhu and Sarah Ostadabbas are with the Electrical and Computing Engineering Department, Northeastern University, USA.

Mackenzi Pergolotti is with the Select Medical, ReVital Cancer Rehabilitation Program, USA.

Smith Giri is with the Department of Medicine, Division of Hematology/Oncology, The University of Alabama at Birmingham, USA.

Hoda Salsabili and Miad Faezipour are with the School of Engineering Technology, Electrical and Computer Engineering Technology, Purdue University, USA.

S. Abdollah Mirbozorgi is with the Electrical and Computing Engineering Department, The University of Alabama at Birmingham, Birmingham, AL 35294 USA (e-mail: samir@uab.edu).

Digital Object Identifier 10.1109/TBME.2023.3253061

0018-9294 © 2023 IEEE. Personal use is permitted, but republication/redistribution requires IEEE permission.
See <https://www.ieee.org/publications/rights/index.html> for more information.

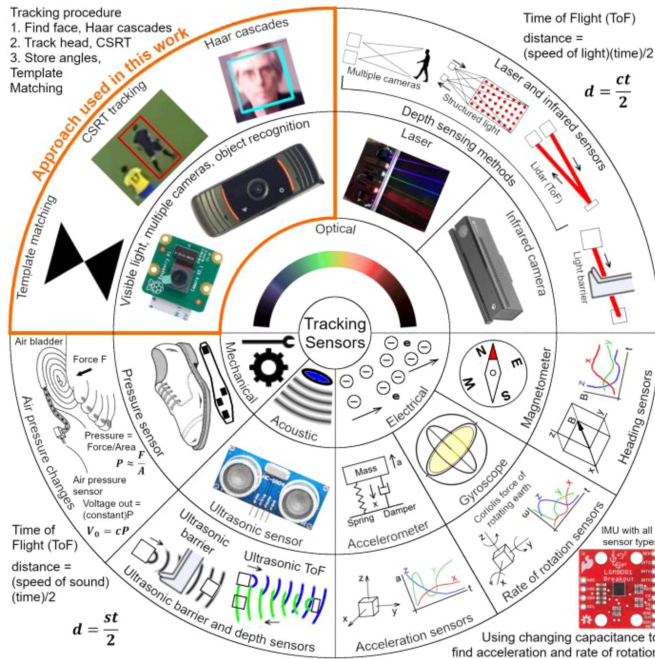


Fig. 1. Review of different technologies for gait speed, standing balance, 5TSS, and TUG tests: top-left) the camera-based design of this work including Channel and Spatial Reliability Tracking (CSRT), Raspberry Pi camera V2.1 [19]; top-right inner ring) camera and optical sensing systems, lasers [20]; top-right inner ring) infrared camera (Xbox One Kinect) [21]; bottom-left) mechanical and acoustic sensor systems (shoe and air bladder) [18], bottom-left) ultrasonic sensor [22]; and bottom-right) electrical accelerometer, gyroscope, and magnetometer sensors [23].

Some different tracking sensor technologies that can be used for the gait speed test, standing balance test, 5 times sit-stand (5TSS) test, and TUG test, are shown in Fig. 1 (see also the comparisons in Table II). Vision-based systems allow many options for gathering data [11], [12], [13]. Present vision-based systems for collecting data use regular cameras [14] and/or infrared cameras [15] for tracking body movements. Camera-based detection systems mainly use fixed setups of multiple cameras and a synchronization processing station, limiting their availability to certain locations. Such systems are expensive and usually operated manually to gather data of various activities from the videos [16]. Other optical devices, shown in Fig. 1 upper right, are designs consisting of multiple cameras or laser units, infrared cameras, or Lidar sensors, which usually are fixed in different parts of a room and are limited to certain locations [17].

In the force-based mechanical approaches, shown in Fig. 1 lower left, the sensors in shoes measure ground contact forces (GCFs) and calculate the phases of gait, instead of gait speed, to find abnormalities in a subject's gait [18]. Additionally, acoustic (ultrasound) sensors are used to measure time of flight by detecting the sound reflection for depth or detecting when a subject passes a certain point (Fig. 1, in the lower left) [17].

Microelectromechanical systems (MEMS) have accelerometer, gyroscope, and magnetometer sensors to detect accelerations, rates of rotations, and headings. These types of sensors

(Fig. 1, in the lower right) are great for step counting and useful for analyzing accelerations of body limbs but have the problem of error accumulation when determining displacement. Their accuracy for measurements of gait speed and distance walked are highly dependent on the location of the sensor on the body.

In this work (Fig. 1 upper left), we have proposed a stand-alone Camera-based Body Motion Tracking (CBMT) system, an automatic and smart device to be used in clinics and hospital for facilitating physical assessment of patients using the SPPB and TUG test. The CBMT system enables human object tracking and recognition, measures all SPPB parameters accurately, is controlled by a smartphone, and can send reports to the cloud to be available to doctors. The RPi operating system can accept security protocols for electronics health record (EHR) systems [24], [25], [26], [27], [28], [29], [30]. In our design, the RPi sends the data to the doctor's laptop/computer without patients' names or other identifying information except for patients' ID numbers. The focus of the proposed work is system development, and clinical trials will be part of our future work, including EHR setup. All experiments are conducted on healthy human subjects with no cancer. The experiments are conducted under IRB 300005372 approved by UAB. The design overview of the proposed system is presented in Section II, including the details of the hardware and software. Section III describes software implementation, and Section IV provides the experimental results. Section V is our discussion (including a comparison of the proposed design with other systems), followed by a conclusion in Section VI.

II. HARDWARE DESIGN AND OVERVIEW

We have used an RPi computer instead of a regular computer to develop a portable and standalone platform. The RPi's are small and can control multiple cameras and motors (without additional hardware) and process all the data. Fig. 2(a) shows the conceptual schematic of the CBMT coverage experimental area, indicating the three tests of gait speed, standing balance, and 5TSS for SPPB, plus the TUG test, that can be measured to evaluate physical performance and to support personalization of cancer treatment among older adults. The best detection range for the CBMT's cameras is 2 m to 7.2 m with 60° viewing angle. It can rotate 180° horizontally with a total view angle of 240°. The system can adjust the cameras vertically if needed ($\pm 20^\circ$), too. The proposed CBMT system's hardware and software functionality connection flow (block diagram) is shown in Fig. 2(b). The two main parts of the hardware are 1) the camera platform system (Raspberry Pi computer, motors, and cameras) and 2) the cell phone. The cell phone can run the RPi remotely and control the system. The hardware of the proposed CBMT platform design consists of 1) one RPi 3B+ computer with 1 GB of RAM, 2) two DC motors, 3) two driver boards (L9110H) for the motors, 4) two USB cameras (ZEALINNO 1080P Webcam), 5) one Raspberry Pi V2.1 camera module, 6) a few acrylic sheets for assembling the components, 7) two camera fine adjustment pieces, and 8) a tripod. This hardware provides all needed functionalities (with the processor, cameras, and mechanical rotation mechanism) to record multiple videos

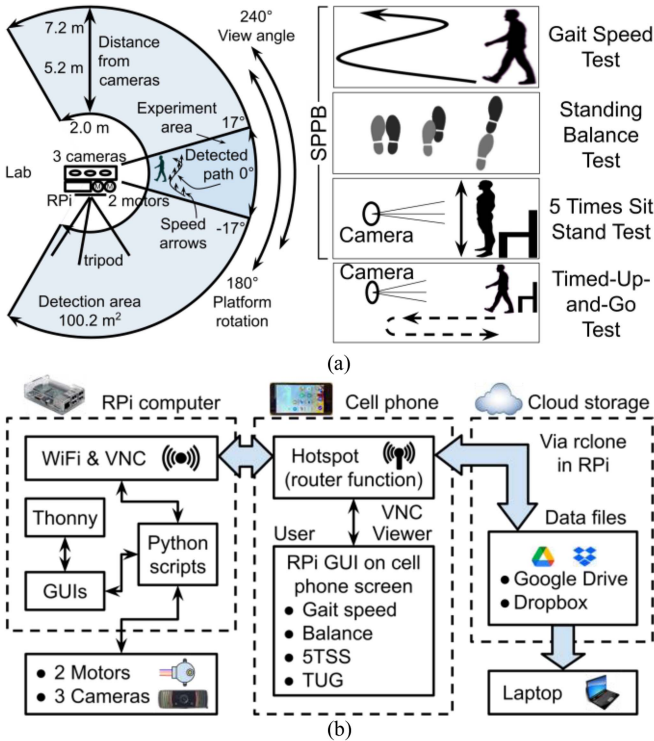


Fig. 2. (a) Experiment area with gait speed, standing balance, 5TSS, and TUG tests, and (b) the proposed Camera-Based Body Motion Tracking (CBMT) system's hardware and software functionality connection flow (block diagram).

for required image processing for gait speed, standing balance, 5TSS, and TUG calculation.

The picture of the implemented CBMT platform with Raspberry Pi, cameras, and motors is shown in Fig. 3. The physical dimensions of the CBMT platform equal 13 cm × 19 cm × 36 cm (without the tripod and marker). The gap between the left and right cameras equals 273.5 mm to detect the depth more accurately. A fixed marker (under the platform, protruding out 18 cm) is used to calculate the overall angle of the subject (regardless of the platform rotation angle), as shown in Fig. 3 inset, by adding the camera platform angle to the subject angle relative to the center of the camera view. The CBMT system uses template matching to find the marker and adjust the platform angle left/right or up/down [31]. This marker is located underneath the moving part of the platform and appears in the center camera image (not blocking the subject in left and right camera views). Multiple markers can be used if the experiment area needs 180° rotation of the platform.

III. SOFTWARE DESIGN AND IMPLEMENTATION

A. Software in RPi

The hardware overview in Fig. 2(b) shows internal functions and software of the proposed and implemented CBMT system. Within the Raspberry Pi block in Fig. 2(b), we have used Thonny, a convenient integrated development environment, to edit and launch Python scripts. The graphical user interfaces (GUIs) are

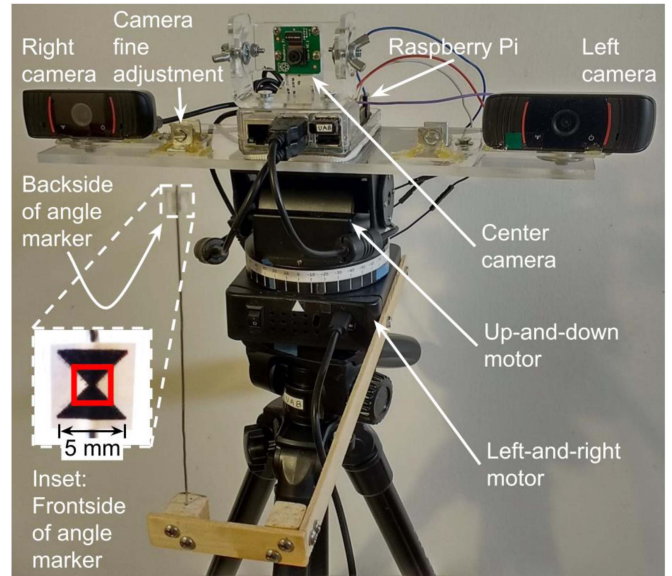


Fig. 3. Implemented platform with Raspberry Pi 3B+, 3 cameras, and 2 DC motors. Inset: the angle marker for platform angle detection mechanism. Software shows detection with red rectangle.

also designed as Python scripts using the tkinter (Tk interface) module. In addition, we have used Rclone, a command line program, to copy files to cloud storage and make the data readily available online [32]. In our design, the Virtual Network Computing (VNC) Server and VNC Viewer are installed in the RPi as a graphical desktop-sharing system. The VNC Server on the RPi works with VNC Viewer on a cell phone to allow viewing of the RPi Desktop on the cell phone screen [33]. The cell phone is merely the interface platform that remotely controls the CBMT system and collects data to store in Dropbox and Google Drive. The image/data processing is done in the RPi, and only the results are delivered and shown in the cell phone. The cell phone can access any data, image, or video files in the RPi remotely.

We have developed a multifunctional software for the proposed CBMT system based on 1) Python3 programming language (version 3.7.3), 2) OpenCV (cv2) library of programming functions primarily for computer vision (version 3.4.6), 3) Imutils image processing functions (version 0.5.3), 4) Channel and Spatial Reliability Tracking (CSRT) function from within OpenCV, 5) tkinter module in Python for creating GUIs, 6) Thonny development environment in the RPi, 7) VNC Server and Viewer in the RPi and cell phone, respectively, 8) Rclone command line program, and 9) RPi.GPIO library for General Purpose Input-Output through the pins on the Raspberry Pi. The software overview is shown in Fig. 4. This overview gives steps used for the cases of gait speed, standing balance, 5TSS, and TUG tests.

B. Cell Phone and Graphical User Interfaces

To connect the RPi to the cell phone (for remote control of the CBMT) VNC is used via the cell phone Wi-Fi hotspot. The GUIs (control GUI and camera GUI) in the RPi appear

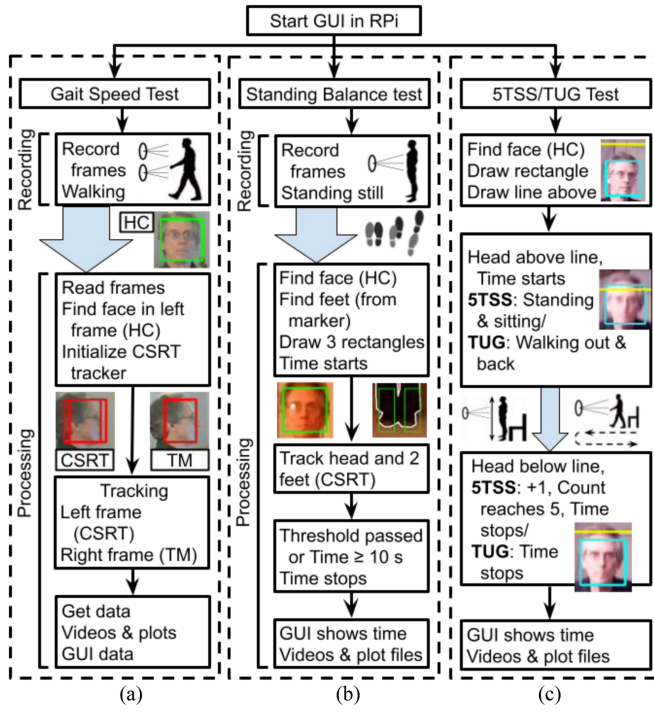


Fig. 4. Software flowchart of camera-based tracking system using template matching (TM), Haar cascades (HC), and Channel and Spatial Reliability Tracking (CSRT) types of object recognition: (a) gait speed test, (b) standing balance test, and (c) 5TSS test/TUG test.

on the cell phone and both GUIs are responsive to touch (the cell phone is the remote monitor, keyboard, mouse, and router of the RPi). The layout of the designed control GUI, including a menu with gait speed, standing balance, 5TSS, and TUG, is shown in Fig. 5(a). The buttons on the control GUI allow 1) running tests, 2) displaying results on the phone, and 3) saving data in comma-separated values (CSV) files. For gait speed, standing balance, 5TSS, and TUG tests, data is kept for doctor's name, patient's ID, time stamp, and elapsed time. In the case of gait speed additional data is kept for walking distance, walking distance error, average speed, and average of errors in a series of runs. There is also a button "Sync data to Google Drive & Dropbox" to upload all result files to those cloud platforms to make them easily accessible. There are also five Help buttons. The results are shown in the control GUI, as well as being saved in CSV files, and being sent to the cloud by pushing one button. There are also buttons to delete video and plot files and data for runs.

The camera GUI, shown in Fig. 5(b), is designed for adjusting the angles of the camera platform using motors. The first and second buttons turn the platform a desired amount based on the angle number entered to the entry box. The third and fourth buttons are designated for fine-tuning the direction of the platform to an angle relative to the marker. This option also displays the horizontal and vertical angle axes of the platform relative to the marker (see Fig. 5(b) inset showing axis degree numbers 0, 20, and 30). This process is needed to set up the system and make it ready to start a new experiment. Fig. 5(c) shows the control GUI when using a cell phone for control.

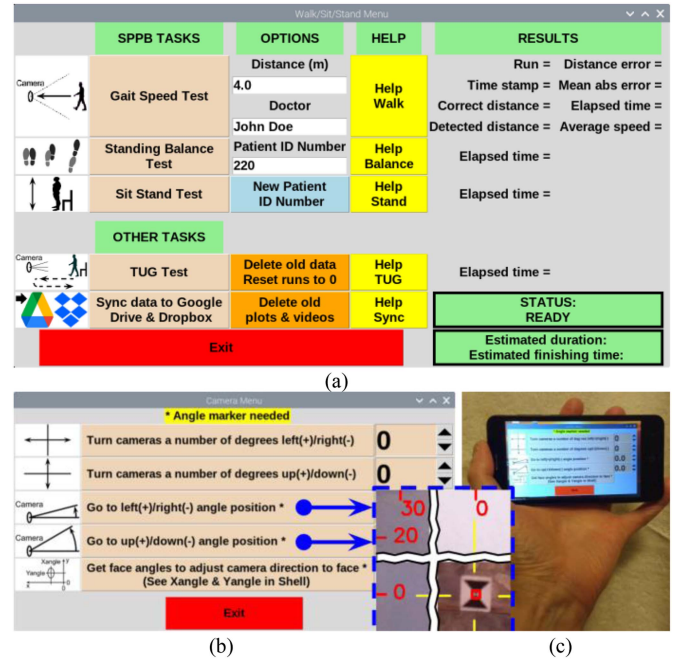


Fig. 5. (a) Control GUI for walk/sit/stand menu, (b) camera menu and inset with degree axes on left and top with cameras centered horizontally and vertically on angle marker, and (c) case of control through cell phone.

C. Object Recognition Techniques

Three different object recognition (object detection) techniques are used in this work: template matching (TM), Haar cascades (HC), and Channel and Spatial Reliability Tracking. This template matching algorithm only requires one photo to use as a template to search for a specific pattern of same size and orientation within an image. It calculates the best match using a squared difference correlation algorithm. A grayscale template T iterates over a grayscale image I in all possible positions where it fits inside. The template is each time compared with the part of the image that it covers. For each upper left corner position (x, y) , it calculates a sum $R(x, y)$ of squared differences of pixel values. By using the method TM_SQDIFF in the OpenCV function, matchTemplate() [34], [35],

$$R(x, y) = \sum_{x', y'} (T(x', y') - I(x + x', y + y'))^2 \quad (1)$$

where (x, y) is the pixel location in the image for a sum, $R(x, y)$ is a sum, $T(x', y')$ is a pixel value of the template, $I(x + x', y + y')$ is a pixel value of the image, and (x') and (y') are the changing coordinate values for making a sum. The pixel location (x, y) where the $R(x, y)$ sum is a minimum is the best match for the template location in the image [34], [35]. We have used the template matching technique to find the fixed angle marker to determine the angle of the camera platform in relation to the marker, as shown in Fig. 3. Template matching is also used to find the position of the subject's head in the right frame when calculating the trajectory in a gait speed test.

The second object recognition technique, Haar cascades, is used to enable searches for more general patterns (human face). Haar cascades uses machine learning to create Haar cascade XML classifier files that contain the classifying training. The cv2 module has methods to find the desired object, a face, at different scales with same orientation [36], [37]. In machine learning the training of a model is done by providing many known positive images that have a face and many known negative images without a face [37]. Many simple Haar features, also known as weak learners, are found in the images [36]. Haar features come from looking at adjacent rectangular areas, summing the intensities of each, and taking the differences of the sums. Integral images simplify these calculations by setting up new pixel values that allow fast summations of pixel values in rectangles of any size [38].

A machine learning process called AdaBoost is used to combine these features into more complex ones, by applying weights and adjusting them until they are the most accurate in classifying each pixel as a face location or not for a given size face [36], [39]. The weights are applied in a model, the XML file, to evaluate new images to find faces and their locations. The word cascades is used because there are multiple filtering passes that start off light to eliminate large areas of the image and progress with more features and accuracy until a face is found [36].

The utilized Channel and Spatial Reliability Tracking object recognition technique in the OpenCV library is a C++ implementation of the CSR-DCF (Channel and Spatial Reliability of Discriminative Correlation Filter) tracking algorithm [40]. The CSRT tracker trains the compressed features of Histogram of Oriented Gradients (HOG) and color names (colornames) by using a correlation filter [41]. In neural networks, compressed features are the resulting features or dimensions after unnecessary features have been removed [42]. The HOG is the gradients of light intensity and their directions/orientations. The gradients will be higher at edges [43]. The colornames is a mapping from pixels values to color names which is used to get features for matching colors [44]. The CSRT tracking is initialized by the selection of a region containing the subject's face in a frame of a video. In the following frames, a search is made near the same region by looking for features of color patches with their edges of the object and its region found in the previous frame. It makes the process faster by not searching the whole frame [41].

D. SPPB Tests Plus TUG Test

We have implemented 3 algorithms to measure all SPPB tests and shown the associated flowcharts in Fig. 4, using the object recognition techniques. It is worth mentioning that we can assess the balancing performance based on the subject's first step or standing performances during the gait speed, 5TSS, or TUG tests.

Gait Speed Test:

1) First Stage: Recording Videos: The left and right cameras are used for recording the gait speed test. In the recording stage, at the start, the subject's head faces the cameras, and the subject begins walking along a predetermined path. It is recorded to two files.

2) Second Stage: Processing Video Frames for Gait Speed and Trajectory Calculation: In the processing stage, frames are read in from the two video files recorded by the left and right cameras. Initialization of a CSRT tracker is done when the face is found in the left frame by using the Haar cascades file. To enable Haar cascades to find the face at a distance of 6 m or 7.2 m, the pixel frame width and frame height of the left frame are both increased by threefold. After that the CSRT tracker keeps the pixel locations of the face or head updated in the left video frames, but CSRT does not need any increased resolution. For each frame pair from initialization until the end, the subject pixel location in the right frame is found by using a template from the left frame and finding a match in the right frame by using template matching.

The left and right cameras are pointed in a nonparallel direction to a point at 4 m distance. This allows the subject to stay more in the center of each frame. A pixel adjustment is added/subtracted to the subject pixel position for the left/right frames, respectively, to correct for the cameras not being parallel. The pixel locations of the subject from the left and right cameras are filtered with customized median filters and moving average filters. The algorithm uses a minimal amount of filtering to remove noise and extra distance due to side-to-side swaying of the subject. The filter length rises from a minimum of 8 data points at the start and finish of the data sequence to a maximum going inward. For a 4-second walk the maximum filter lengths are 21 and 55 for radial and crosswise gait speed, respectively. For a 20-second walk the maximum filter lengths are 51 and 255 for radial and crosswise gait speed, respectively. The low filtering near the end points protects data of end points, and the filtering in general results in a more accurate calculation of the distance moved. In our previous work, we have provided the method of using triangulation technique to obtain polar coordinate positions from subject pixel position pairs [31]. To minimize the depth inaccuracies of the gait speed calculation, we have calibrated the system with (2) and (3), which are based on fitting cubic equations to given data. Angle and distance data were created from 64 locations on an 8-by-8 rectangular grid that covers the experiment area. Equation (2) is the creation of a function.

$$\text{depth_f} = \text{interp2d}(X, Y, R, 'cubic') \quad (2)$$

where depth_f is a function being created to obtain correct depth, interp2d is a Python function for 2D interpolation, X and Y are lists of rectangular coordinates for detected depths and angles, R is a list of correct depths that correspond to the other two lists, and 'cubic' is a string specifying the type of interpolation. The correct depth for a single case is calculated in (3).

$$\text{dep} = \text{depth_f}(x, y) \quad (3)$$

where dep is a correct depth, and x and y are rectangular coordinates for a detected depth and angle.

Standing Balance Test: To evaluate the standing balance, first, the center camera records the subject standing still. The standing balance test requires the subject to stand with the feet together in side-by-side, semi-tandem, and tandem positions. For each of the three cases the subject must stand for 10 seconds without

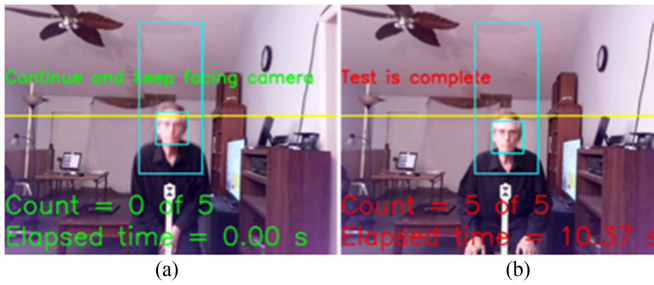


Fig. 6. 5 times sit-stand test. (a) Head rises above yellow line and timer starts. (b) Head falls below yellow line for fifth time and timer stops.

moving the feet or the head [45], [46]. There is an option to ignore head movement when having the test.

In preparation it is necessary to mark the floor with masking tape at 3.5 m for a feet location marker and at 4 m camera distance for the standing position. The cameras are pointed at the person's crotch. Pixels are automatically trimmed on the left and right of the frame to center the subject in the view, and to increase the frame rate. From the video recording, the developed code detects the face of the subject with Haar cascades. By using template matching to find an angle marker (see Fig. 10(a)), the relative positions of the left and right feet are found. For the tandem position the subject stands with feet at a slight angle toward the side of the forward foot so that both feet are visible to the camera. There are three CSRT tracking boxes for the head [47], the left foot, and the right foot, to get data, as shown in Fig. 4(b). Each foot tracker tracks within its own independent yellow frame (Fig. 10(a)) to avoid interference from the other foot. The software will detect if one of these three body parts moves more than the distance thresholds (feet: >25 mm, head: >35 mm) that are set (see Fig. 10). Movements are represented by horizontal x-type and vertical y-type curve labels. The evaluation results can be classified as Pass and Fail scores or by giving scores in a numerical range (e.g., 1–10). The test will give a result of 10 or more seconds for a success and a result of less than 10 seconds for a failure or partial success. The average frame rate is 22 frames per second (fps) and the time resolution is under 0.055 s for standing balance tests.

5 Times Sit-Stand Test: The 5TSS test algorithm finds elapsed time for the subject to stand and sit 5 times. Fig. 6 shows prompts for the test that the user and subject can view. The software detects the level of the top of the face with Haar cascades and adds one to the count each time the subject stands and sits. The average frame rate is 25 frames per second (fps) and the time resolution is under 0.050 s for 5TSS tests.

Timed Up and Go Test: The TUG test finds elapsed time for the subject to stand from a standard armchair, walk 3 m forward, turn around, walk 3 m back, turn around again, and sit back down. It also uses Haar cascades to detect the level of the top of the face. The user and subject can view the prompts for the test. The average frame rate is 27 frames per second (fps) and the time resolution is under 0.050 s for TUG tests.

Codes for This Project: All the codes developed for this project are shared in Zenodo [48].

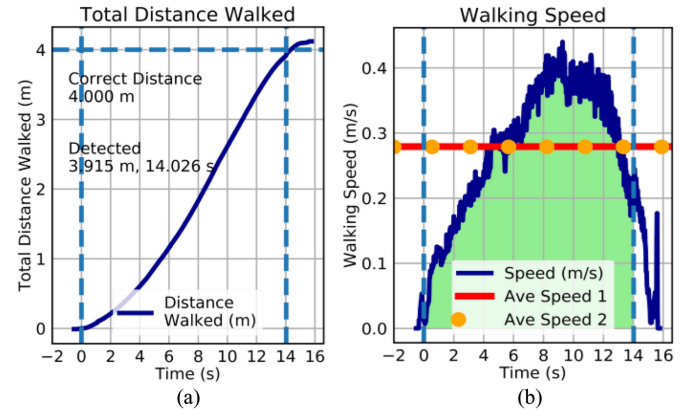


Fig. 7. Plots of (a) total distance walked with blue vertical lines marking start and finish and (b) walking speed with Ave Speed 1 (average speed from distance (red line)) and Ave Speed 2 (average speed from speed area (orange dots)). Speed area is green.

IV. EXPERIMENTAL RESULTS, SPPB

Human Subject Population and Testing Environments: We have conducted all experiments on healthy subjects with no cancer within two subject groups of young and old adults. The implemented CBMT platform, shown in Fig. 3, is used to conduct in vivo experiments with a subject population of 8 human volunteers, 4 with ages 60–95, 3 males and 1 female, all light complexions; and 4 with ages 22–42, 3 males and 1 female, 3 with light complexions and 1 with a dark complexion. The total 69 test runs were done with a lighting range of 20–430 lux, measured by a digital lux meter (LX1330B), which is beyond the standard illumination for hospitals/clinics, 150–300 lux [49]. We have used the same CBMT system for all SPPB tests. The system is equipped with a battery power bank that can work continuously for 8 hours. By turning the CBMT system on, it takes less than 45 s to be initialized and be ready to execute tests. The operator was also the subject of some of the experiments, indicating the simplicity of conducting tests using the CBMT system.

Results, Gait Speed Test: The distances walked and walking speeds for a gait speed test are shown in plots in Fig. 7, measured by the CBMT prototype. The two vertical light blue lines in Fig. 7(a) mark the start and end of timing for the walk. The software generates the lines automatically by analyzing the changes in angle over time. The curve in Fig. 7(a) is smooth and advances steadily, indicating that the subject had good balance and did not falter or pause while walking. A minimal amount of filtering to remove noise was used. The subject walked slowly and took about 14 s to walk 4 m. The measured instantaneous walking speed is shown in Fig. 7(b). The walking speed naturally starts slowly, reaches higher levels in the middle of the plot, and drops back down at the finishing time. The red horizontal line for average speed (Ave Speed 1) is obtained by dividing the total distance walked by the total time. The orange horizontal dotted line for average speed (Ave Speed 2) is obtained by first taking the green area under the curve as the total distance. The average speed (Ave Speed 2) is found by dividing the total distance by

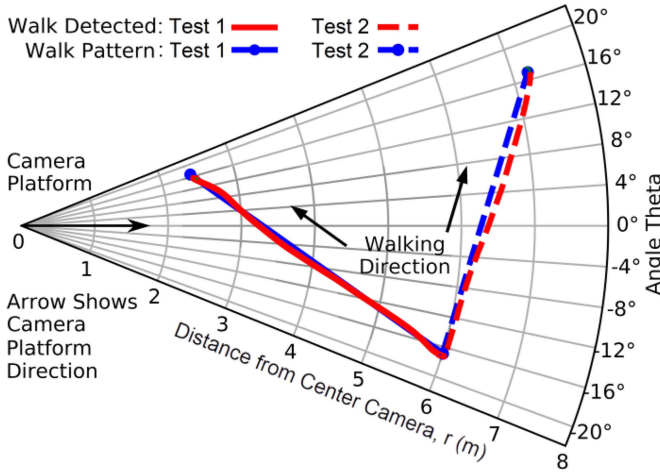


Fig. 8. Plot of detected walking trajectories for Test 1 (walking toward cameras) and for Test 2 (walking crosswise).

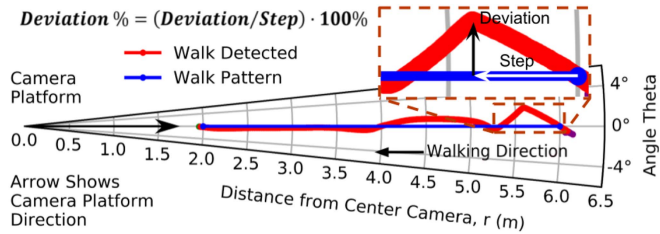


Fig. 9. Gait speed trajectory showing lack of balance with unsteady 40 cm first step 20 cm to the right. See expanded inset (deviation % = 50%). This was a special case with lower filtering.

the total time, shown in (4),

$$\text{AveSpeed2} = \frac{\sum_{i=1}^{n-1} [(t_{i+1} - t_i)(s_i + s_{i+1}) / 2]}{\text{total time}} \quad (4)$$

where t is time, s is speed, and there are n values of each labeled with the subscripts i and $i+1$.

Polar plots for trajectories walking toward the cameras and walking crosswise are shown in Fig. 8.

Results, Standing Balance Test: Measurement results for standing balance tests are shown in the plots of Fig. 10(b) and (c). For the head, left foot, and right foot, the horizontal (x-type label) and vertical (y-type label) movements in millimeters of each are measured and plotted. In Fig. 10(b) the subject stands still successfully for over 10 s. In Fig. 10(c) the subject moves a foot to the left, and is credited with standing still for 4.67 s. Because there is a small amount of jitter detected even when standing perfectly still, a distance threshold is used to judge whether or not the subject moved.

Poor Balance Seen with Other Tests: Poor balance can be detected in the 2D polar plot of a crooked detected gait speed walking path as shown in Fig. 9. The subject faltered deliberately by taking an unsteady first step 20 cm to the right. A calculation of *deviation percent (%)* for the first step (normalized to first step size) and shown in Fig. 9 (with a deviation percent of 50%), can be used to estimate unbalanced level. It should be noted that

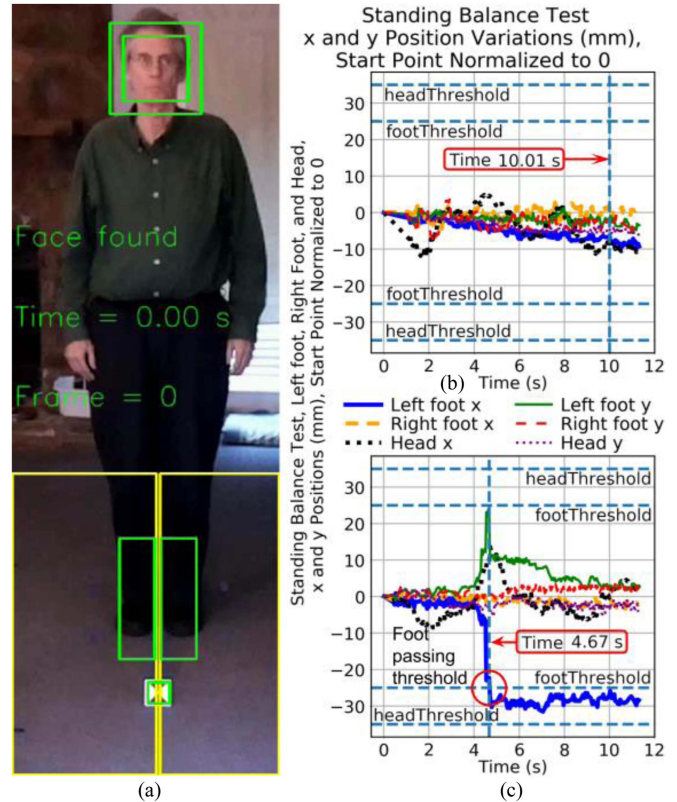


Fig. 10. Measured standing balance test with (a) video showing three green tracking boxes (head: outer green box, feet: lower green boxes), two yellow independent frames in the bottom for feet trackers, and small green box around a marker at bottom for initial location of feet; (b) plot for successful stand for over 10 s; and (c) plot for failing stand of 4.67 s because the foot viewed on the left moved about 30 mm to the left. (See the thick blue *L* *foot x* curve where it crosses the foot threshold at -25 mm (marked with a red circle)).

the filtering level in Fig. 9 was a special case as it was lower than the filtering level used in the runs shown in Table I.

A lower deviation percent (under 20% for example) can be considered as a normal shifting of the weight when walking slowly. The trajectory straightens out as the subject gains speed walking toward the cameras. Poor balance can also be detected from an uneven sitting and standing plot on the 5TSS test. A 5TSS test plot is shown in Fig. 11(a), illustrating good balance, because the standing durations are fairly equal and done in a short time.

Results, 5 Times Sit-Stand Test: In Fig. 11(a) is shown a normalized plot (the height of the top of the subject's face) for a 5TSS test as a function of time. Fig. 11(a) is the measured results of a 5TSS test, using the same human subject. The subject performed the test smoothly as shown by the 5 smooth rises and falls of the evenly spaced curve. There is a natural head position adjustment after each time sitting (due to leaning back in the chair). A brown oval marks one of these in the lower part of the plot.

Human Subject Population Results (Table I, Figs. 12, and 13): The implemented CBMT platform is used to collect data for the gait speed, standing balance, 5TSS, and TUG tests in several

TABLE I

SUMMARY OF THE MEASURED RESULTS OF THE PROPOSED CBMT SYSTEM FOR SUBJECT POPULATION OF 8 VOLUNTEERS AND 69 TEST RUNS

Type of Test	Frame Rate (frames/s), Resolution (pixels)	Average Speed Range (m/s)	Gait Speed Resolution (m/s)	Distance (m) / Time Range (s)	Average Accuracy
Gait speed, Crosswise, 8 subjects, 17 runs, Fig. 8	53, 640x96 x 2 frames = 122,880	0.191 to 1.259	<0.127	2.832 to 3.836 / 2.75 to 20.06	Distance accuracy: 95.28%
Gait speed, Radial, 1 subject, 8 runs, Fig. 8	39, 640x144 x 2 frames = 184,320	0.136 to 1.371	<0.067	3.866 / 2.82 to 28.35	Distance accuracy: 97.47%
Standing balance (3 types), 8 subjects, 18 runs, Fig. 10	22, 304x848 = 257,792	N/A	N/A	0.0 / 0.75 to 10.09	Time accuracy: 97.25%
5 Times Sit-Stand, 7 subjects, 11 runs, Fig. 11a	25, 400x480 = 192,000	N/A	N/A	0.0 / 6.93 to 16.94	Time accuracy: 99.10%
Timed Up and Go, 7 subjects, 15 runs, Fig. 11b	27, 480x480 = 230,400	N/A	N/A	6.0 / 6.82 to 14.28	Time accuracy: 98.38%

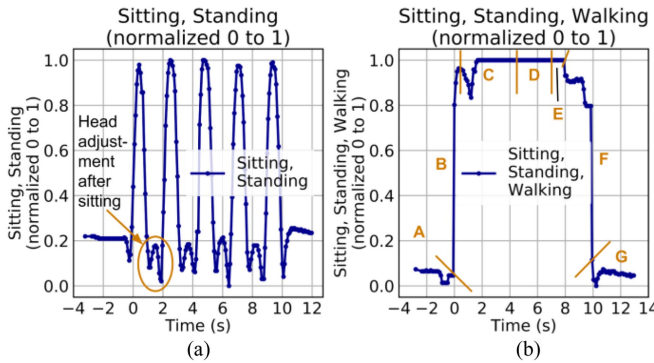


Fig. 11. (a) 5 times sit-stand test with sitting and standing normalized 0 to 1, and (b) Timed Up and Go test with sitting, standing, and walking normalized 0 to 1. The labels A–G indicate different phases of TUG.

runs to evaluate the accuracy and consistency of the system. The measured results of all the tests are shown in Table I. There are 25 runs for gait speed walking, 17 runs along a line crosswise in relation to the cameras and 8 runs along a line toward the cameras. The first data column includes the information of frame rates and obtained resolutions (pixel sizes) for all the tests. The second data column shows the measured average gait speed ranges for 25 runs in total. The measured gait speed resolutions are reported in the third data column. The gait speed resolution for each run was calculated by multiplying the absolute value of the decimal error by the average speed. The distances walked and time ranges for the walks are shown in the second to last column. There is no walking in the standing balance or 5TSS tests. The TUG test is a combination of sitting, standing, and walking. The subject stands from a chair, walks 3 m toward the cameras, walks 3 m back to the chair, turns, and sits. The last data column indicates the measured averages of distance accuracies for the gait speed tests, >95%, and time accuracies for the other tests, >97%.

Confidence Intervals (95%) for Physical Test Errors

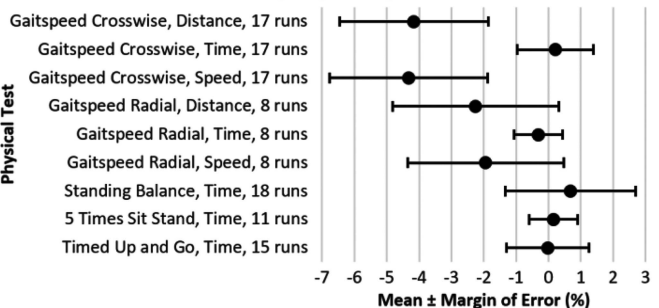


Fig. 12. Plot of 95% confidence intervals for percent errors of distance, time, and speed in gait speed tests (two types), and percent errors of time in standing balance, 5 times sit-stand, and Timed Up and Go tests. A stopwatch and measured floor distances were used as references.

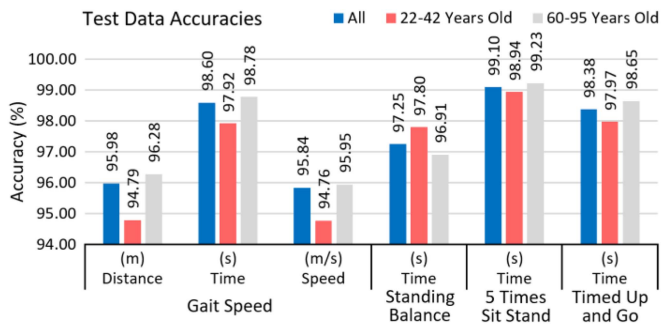


Fig. 13. Bar graphs of distance, time and speed accuracies for gait speed tests, and time accuracies for standing balance, 5 times sit-stand, and Timed Up and Go tests. Accuracies for age groups younger, older, and for all are shown.

In Fig. 12 are shown the 95% confidence intervals for errors in distance, time, and average speed for gait speed tests and time errors in standing balance, 5 times sit-stand, and Timed Up and Go tests. Fig. 13 shows the accuracies of test data for younger and older age groups, and for all. Differences between age groups are small.

V. DISCUSSION (TUG TEST AND COMPARISON)

In this section, we present a discussion about the Timed Up and Go test and compare the performance of the proposed CBMT system with the commercialized technologies and state-of-the-art published works.

Results, Timed Up and Go Test: In Fig. 11(b) is shown a normalized plot (the height of the top of the subject's face) for a TUG test as a function of time. The different stages of the TUG test shown in Fig. 11(b) (measured TUG results) are labeled with the brown letters A through G, in which each letter is associated with an activity and time range. The stages are as follows: A: sitting (-3 s to 0 s), B: standing up (0 s to 0.5 s), C: walking toward cameras (0.5 s to 4.5 s), D: walking back to the chair (4.5 s to 7.0 s), E: turning around to face cameras (7.0 s to 8.0 s), F: sitting down (8.0 s to 9.9 s), and G: sitting (9.9 s to 13.1 s). There is head adjustment after standing and before sitting shown by jitters in the curve at the start of C and at the start of F, but the whole test was done without faltering. The jitters are due to

TABLE II
COMPARISON OF TECHNOLOGIES FOR GAIT SPEED, TIMED UP AND GO, AND 5 TIMES SIT-STAND TESTS

Name/Tech/ Company/ Reference Parameters	AMP331 (D.I. Inc.) [51], [52]	UltraGait Speed v2.0 [53]	IMU (on feet) [54]	Gaitspeedometers 4 Types [17]	MetaWear CPro sensor [55]	Microsoft Kinect V2 [56]	Microstrain 3DM-GX1 [57]	Unsupervised Screening System [58]	APDM ML system (version 2) [59], [50]	This Work (69 test runs)
Sensor Type	Accelerometer	Ultrasonic	IMU	Laser, infrared, ultrasonic	IMU	Camera, infrared	IMU	LB, aTUG, IMU, camera	IMU	Visible-light cameras
Gait Speed Test	YES	YES	YES	YES	YES	YES	NO	NO	YES	YES
Distance Acc/Err (%)	97% to 99% Ave Acc	-	-	-	97.57% & 89.3% Ave Acc	-	N/A	N/A	-	95.98% Ave Acc
Gait Speed Acc/Err (%)	-	-	85.59% Ave Acc	98.3%, 86.1%, 98.6%, 95.9% Ave Acc	97.57% & 89.3% Ave Acc	-	N/A	N/A	ICC = 0.928	95.84% Ave Acc
Time Acc/Err (%)	-	4.13% and 7.39% ARE	-	98.3%, 86.1%, 98.6%, 95.9% Ave Acc	99.01% Ave Acc	-	N/A	N/A	-	98.59% Ave Acc
Coverage Area (m, m ²)	18 m ²	4 m	~83 m	4 m	~38 m	3 m	5 m	~3.5 m	6 m x 0.6 m	2 to 7.2 m, 60° view
Standing Balance Test	NO	NO	NO	NO	NO	NO	NO	NO	YES	YES
Time (s) Acc/Err (%)	N/A	N/A	N/A	N/A	N/A	N/A	N/A	N/A	-	97.25% Ave Acc
5 Times Sit- Stand Test	NO	NO	NO	NO	NO	NO	NO	YES	NO	YES
Time (s) Acc/Err (%)	N/A	N/A	N/A	N/A	N/A	N/A	N/A	LB CC 0.73 IMU CC 0.87	N/A	99.10% Ave Acc
TUG Test	NO	NO	NO	NO	NO	YES	YES	YES	NO	YES
Time (s) Acc/Err (%)	N/A	N/A	N/A	N/A	N/A	Ave diff 0.001 s	Ave diff of mean 2.99 %	LB CC 0.89 IMU CC 0.78	N/A	98.38% Ave Acc
Data Handling	USB, Wireless	Bluetooth, phone, cloud	Bluetooth, smartphone	Phone displays, microcontrollers	Bluetooth, phone	USB	cable, RS-232 or RS-485	RFID, cables	wireless	WiFi, Cloud Storage
Processor	Computer	Computer	Arduino mega 2560	Microcontrollers	Android phone, app	Computer, Kinect V2	Computer, Microstrain, Vicon	Computer	Laptop	Raspberry Pi

Accuracy = $\left(100 - \frac{|TrueValue - MeasuredValue|}{TrueValue} \times 100\right)\%$ [55]; **Tech** = Technology; **AMP331 (D.I. Inc.)** = Activity Monitoring Pod 331 (Dynastream Innovations Inc.); **IMU** = Inertial measurement unit; **APDM ML** = Ambulatory Parkinson's Disease Monitoring MobilityLab/Opal sensors; **LB** = Light barrier sensor; **aTUG** = ambient TUG chair automatically measuring TUG via an infrared Light Barrier, four Force Sensors (on chair), and a Laser Range-Scanner; **Acc/Err** = Accuracy/Error; **ICC** = intra-class correlation coefficients with GAITRite pressure sensor walkway as reference system; **MAE** = Mean Absolute Error = average of absolute values of errors with $MAE = \frac{1}{n} \sum_{i=1}^n |x_i - \bar{x}|$ where n is the number of measured values, \bar{x} is the correct value, and x_i is a measured value (means of system compared with means of Vicon as true); **Ave Acc** = Average Accuracy; **ARE** = Average relative error (%) with respect to manual watch; **Coverage area** = Also distance walked on a treadmill; **Ave diff** = Average TUG test durations differences from those measured by clinicians; **LB CC** = Light barrier sensor correlation coefficient (between it and stopwatch); **IMU CC** = Inertia measurement unit correlation coefficient (between it and stopwatch); **RS-232 or RS-485** = Standards for serial communication transmission of data; **RFID** = Radio-frequency identification; **Vicon** = Camera system being used for comparison.

a natural movement, not from an unbalanced state. In this test, the TUG took 9.9 s to be completed for a healthy adult male, but he was walking at a slower than normal speed. Over 10 s for a top speed would indicate a low physical performance.

Comparisons of Technologies in Table II: Different state-of-the-art technologies for performing gait speed, standing balance, 5TSS, and TUG tests, are compared with the proposed technology, and the results are summarized in Table II. The table focuses on the accuracies or errors of various technologies for the three tests. The AMP331, IMU (on feet), MetaWear CPro sensor, Microstrain 3DM-GX1, Unsupervised Screening System, and APDM ML system/Opal sensors [50], all use Inertial Measurement Units (IMUs) or accelerometers. Some wearable accelerometer-based devices may obtain displacement somewhat accurately after calibration, but there is displacement error accumulation that can affect the accuracy. Accuracy of displacement measurement from IMU devices (based on acceleration and converting it to gait speed) is complicated

and varies depending on the location of the sensors on the body, age of subjects walking, and performance of the IMUs. The UltraGaitSpeed v2.0 and Gaitspeedometers both use ultrasound. Time of flight sensors may use infrared, lasers, or ultrasound to obtain depth of a subject. The Kinect device can detect body postures and uses both infrared and visible light. Devices with infrared cameras can be expensive. The setup of lasers or ultrasound for light barriers is not very mobile.

This proposed work is the only one found to be applied to all three of the SPPB tests and TUG test. The proposed system shows results in the GUI, and uploads test data to the cloud by clicking a button. Data, plots, and videos are produced automatically, and easily removed when no longer needed. For the gait speed measurement tests, we have achieved average accuracy of >95% for distance traveled and average gait speed. The average time accuracies for standing balance, 5TSS, and TUG are measured >97%.

VI. CONCLUSION

We have designed and implemented a camera-based system that can evaluate SPPB for physical assessment of patients with cancer, including gait speed, standing balance, and 5TSS tests. The SPPB and the TUG tests will be conducted to evaluate physical performance. Such data can be used to support personalization of cancer treatment among older adults. We have developed the codes and algorithms/GUIs (CBMT software) for processing the captured images of the three cameras to evaluate SPPB and TUG. We have also equipped the CBMT system with the capability to be remotely controlled via smartphone, accessed easily with GUIs, and work automatically to get data for evaluating physical status of a patient (data is stored in the Raspberry Pi and can be uploaded to the cloud). The 5TSS and TUG tests are done in real time, and the gait speed and standing balance results are ready after test completion and quick processing. By the erratic walking trajectory plot or an uneven plot for 5TSS, the CBMT can estimate the level of steadiness of the standing/walking balance. The proposed work is the only device among those reviewed that does all three SPPB tests (gait speed, standing balance, and 5TSS) and the TUG test. We have conducted in vivo experiments with human subject population of 8 volunteers with a total of 69 test runs, including 4 older people with ages 60–95 (males and female). For the gait speed measurement tests, we have achieved average accuracy of >95% for distance traveled and average gait speed. The average time accuracies for standing balance, 5TSS, and TUG are measured >97%.

REFERENCES

- [1] B. D. Smith et al., "Future of cancer incidence in the United States: Burdens upon an aging, changing nation," *J. Clin. Oncol.*, vol. 27, no. 17, pp. 2758–2765, Jun. 2009.
- [2] K. D. Miller et al., "Cancer treatment and survivorship statistics, 2016," *CA: A Cancer J. Clinicians*, vol. 66, no. 4, pp. 271–289, Jul. 2016.
- [3] H. S. Wu and J. K. Harden, "Symptom burden and quality of life in survivorship: A review of the literature," *Cancer Nurs.*, vol. 38, no. 1, pp. E29–E54, Jan. 2015.
- [4] J. Neo et al., "Disability in activities of daily living among adults with cancer: A systematic review and meta-analysis," *Cancer Treat. Rev.*, vol. 61, pp. 94–106, Dec. 2017.
- [5] M. Pergolotti et al., "Older adults with cancer: A randomized controlled trial of occupational and physical therapy," *J. Amer. Geriatrics Soc.*, vol. 67, no. 5, pp. 953–960, May 2019.
- [6] S. G. Mohile et al., "Practical assessment and management of vulnerabilities in older patients receiving chemotherapy: ASCO guideline for geriatric oncology," *J. Clin. Oncol.*, vol. 36, no. 22, pp. 2326–2347, 2018.
- [7] S. Giri et al., "Impact of geriatric assessment (GA) based frailty index (CARE-frailty index) on mortality and treatment-related toxicity among older adults with gastrointestinal (GI) malignancies," *J. Clin. Oncol.*, vol. 39, no. 15, pp. 12046–12046, May 2021.
- [8] A. P. Marsh et al., "The virtual short physical performance battery," *J. Gerontol. Ser. A: Biomed. Sci. Med. Sci.*, vol. 70, no. 10, pp. 1233–1241, Oct. 2015.
- [9] W. Dale et al., "How is geriatric assessment used in clinical practice for older adults with cancer? A survey of cancer providers by the American Society of Clinical Oncology," *JCO Oncol. Pract.*, vol. 17, no. 6, pp. 336–344, 2021.
- [10] Y. Ezzatvar et al., "Physical function and all-cause mortality in older adults diagnosed with cancer: A systematic review and meta-analysis," *J. Gerontol. Ser. A, Biol. Sci. Med. Sci.*, vol. 76, no. 8, pp. 1447–1453, 2021.
- [11] S. Ostadabbas et al., "A vision-based respiration monitoring system for passive airway resistance estimation," *IEEE Trans. Biomed. Eng.*, vol. 63, no. 9, pp. 1904–1913, Sep. 2016.
- [12] Z. Wang, S. Abdollah Mirbozorgi, and M. Ghovanloo, "An automated behavior analysis system for freely moving rodents using depth image," *Med. Biol. Eng. Comput.*, vol. 56, pp. 1807–1821, Mar. 2018.
- [13] M. Aloudat, M. Faezipour, and A. El-Sayed, "Automated vision-based high intraocular pressure detection using frontal eye images," *IEEE J. Transl. Eng. Health Med.*, vol. 7, no. 1, May 2019, Art. no. 3800113.
- [14] F. Wang et al., "Toward a passive low-cost in-home gait assessment system for older adults," *IEEE J. Biomed. Health Inform.*, vol. 17, no. 2, pp. 346–355, Mar. 2013.
- [15] E. E. Stone and M. Skubic, "Unobtrusive, continuous, in-home gait measurement using the Microsoft Kinect," *IEEE Trans. Biomed. Eng.*, vol. 60, no. 10, pp. 2925–2932, Oct. 2013.
- [16] B. Muñoz et al., "Automated gait analysis using a Kinect camera and wavelets," in *Proc. IEEE 20th Int. Conf. e-Health Netw. Appl. Serv.*, 2018, pp. 1–5.
- [17] H. W. Jung et al., "Cross-comparisons of gait speeds by automatic sensors and a stopwatch to provide converting formula between measuring modalities," *Ann. Geriatr. Med. Res.*, vol. 23, no. 2, pp. 71–76, Jun. 2019.
- [18] K. Kong and M. Tomizuka, "A gait monitoring system based on air pressure sensors embedded in a shoe," *IEEE/ASME Trans. Mechatronics*, vol. 14, no. 3, pp. 358–370, Jun. 2009.
- [19] Seeed Technology Co., Ltd., "Raspberry Pi camera module v2," 2022, [Online]. Available: <https://www.seeedstudio.com/Raspberry-Pi-Camera-Module-V2.html>
- [20] Wikipedia, "Laser," Aug. 2021, [Online]. Available: <https://en.wikipedia.org/wiki/Laser>
- [21] Wikipedia, "Kinect," Jul. 2021, [Online]. Available: <https://en.wikipedia.org/wiki/Kinect>
- [22] SainSmart, "Ultrasonic ranging detector mod HC-SR04 distance sensor," 2023. [Online]. Available: <https://www.sainsmart.com/products/ultrasonic-ranging-detector-mod-hc-sr04-distance-sensor>
- [23] SparkFun Electronics, "SparkFun 9DoF IMU breakout-LSM9DS1." Accessed: 2023. [Online]. Available: <https://www.sparkfun.com/products/13284>
- [24] Epic Systems Corporation, "Open Epic," 2023, [Online]. Available: <https://open.epic.com/>
- [25] R. J. Johnson III, "A comprehensive review of an electronic health record system soon to assume market ascendancy: EPIC," *J. Healthcare Commun.*, vol. 1, no. 4, Sep. 2016, Art. no. 36.
- [26] GnuPG, "GnuPG download," Dec. 2022, [Online]. Available: <https://gnupg.org/download/index.html>
- [27] P. Mahon, "pmahon2016/pgp," Sep. 2020, [Online]. Available: <https://github.com/pmahon2016/pgp>
- [28] S. Pandey et al., "Human performance in Google's two-factor authentication setup process," in *Proc. Hum. Factors Ergonom. Soc. Annu. Meeting*, 2019, pp. 2221–2225.
- [29] Gpg4win, "Gpg4win-a secure solution" Accessed: 2023. [Online]. Available: <https://www.gpg4win.org/>
- [30] GPGTools, "GPG suite," 2023, [Online]. Available: <https://gpgtools.org/>
- [31] L. Duncan et al., "Camera-based human gait speed monitoring and tracking for performance assessment of elderly patients with cancer," in *Proc. IEEE 43rd Annu. Int. Conf. Eng. Med. Biol. Soc.*, 2021, pp. 3522–3525.
- [32] Jarrod, "Project: RaspberryPi Google drive sync," Aug. 2018, [Online]. Available: <https://jarrodstech.net/project-raspberrypi-google-drive-sync/>
- [33] B. Srinivasulu et al., "VNC viewer authentication and security using remote frame buffer protocol," *Int. J. Eng. Res. Appl.*, vol. 3, no. 6, pp. 1007–1011, Nov./Dec. 2013.
- [34] OpenCV, "Template matching," 2019. [Online]. Available: https://docs.opencv.org/3.4.6/de/da9/tutorial_template_matching.html
- [35] A. Basulto-Lantsova et al., "Performance comparative of OpenCV template matching method on Jetson TX2 and Jetson Nano developer kits," in *Proc. IEEE 10th Annu. Comput. Commun. Workshop Conf.*, 2020, pp. 812–816.
- [36] P. Viola and M. Jones, "Rapid object detection using a boosted cascade of simple features," in *Proc. IEEE Comput. Soc. Conf. Comput. Vis. Pattern Recognit.*, 2001, pp. I/I.
- [37] OpenCV, "Face detection using Haar cascades," 2019, [Online]. Available: https://docs.opencv.org/3.4.6/d7/d8b/tutorial_py_face_detection.html#gsc.tab=0
- [38] C. Rahmad et al., "Comparison of Viola-Jones Haar cascade classifier and histogram of oriented gradients (HOG) for face detection," in *Proc. IOP Conf. Ser.: Mater. Sci. Eng.*, 2020, Art. no. 012038.

- [39] R. Wang, "AdaBoost for feature selection, classification and its relation with SVM, a review," *Phys. Procedia*, vol. 25, pp. 800–807, 2012.
- [40] K. Farkhodov et al., "Object tracking using CSRT tracker and RCNN," in *Proc. 7th Int. Conf. Bioimaging*, 2020, pp. 209–212.
- [41] A. LuNežić et al., "Discriminative correlation filter tracker with channel and spatial reliability," *Int. J. Comput. Vis.*, vol. 126, pp. 671–688, Jan. 2018.
- [42] P. Taylor et al., "Feature selection for supervised learning and compression," *Appl. Artif. Intell.*, vol. 36, no. 1, 2022, Art. no. e2034293.
- [43] N. Dalal and B. Triggs, "Histograms of oriented gradients for human detection," in *Proc. IEEE Conf. Comput. Vis. Pattern Recognit.*, 2005, pp. 886–893.
- [44] J. V. D. Weijer and F. S. Khan, "An overview of color name applications in computer vision," in *Proc. 5th Int. Workshop Comput. Color Imag.*, 2015, pp. 16–22.
- [45] Frailty Science, "Short physical performance battery (SPPB) as a frailty measure." Accessed: 2023. [Online]. Available: <https://frailtyscience.org/sites/default/files/2020-09/Frailty%20Assessment%20Definition%20Sheet%20-%20SPPB%20as%20a%20frailty%20measure.pdf>
- [46] Centers for Disease Control and Prevention (CDC), "The 4-stage balance test." 2017. [Online]. Available: https://www.cdc.gov/steady/pdf/4-Stage_Balance_Test-print.pdf
- [47] A. Al-Rahayfeh and M. Faezipour, "Eye tracking and head movement detection: A state-of-art survey," *IEEE J. Transl. Eng. Health Med.*, vol. 1, 2013, Art. no. 2100212.
- [48] L. D. Duncan, "Raspberry Pi camera tracking," Feb. 2023. [Online]. Available: <https://zenodo.org/badge/latestdoi/590297493>
- [49] BFW, Inc., "Hospital lighting guide & standards," Oct. 2019. [Online]. Available: <https://www.bfwinc.com/hospital-lighting-standards/#:~:text=In%20a%20physiological%20examination%20room,illumination%20here%20is%20150%2D300lx>
- [50] P. C. Fino et al., "Postural sway, falls, and self-reported neuropathy in aging female cancer survivors," *Gait Posture*, vol. 69, pp. 136–142, Jan. 2019.
- [51] C. C. Yang and Y. L. Hsu, "A review of accelerometry-based wearable motion detectors for physical activity monitoring," *Sensors*, vol. 10, pp. 7772–7788, 2010.
- [52] L. Edbrooke et al., "Can an accelerometer-based monitor be used to accurately assess physical activity in a population of survivors of critical illness?," *Glob. J. Health Sci.*, vol. 4, pp. 98–107, May 2012.
- [53] X. Ferre et al., "Gait speed measurement for elderly patients with risk of frailty," *Mobile Inf. Syst.*, vol. 2017, pp. 1–11, Dec. 2017.
- [54] Y. C. Huang et al., "Wearable sensor for measurement of gait walking and running motion," *Sensors Mater.*, vol. 31, no. 2, pp. 629–644, Feb. 2019.
- [55] A. R. Anwary et al., "An automatic gait feature extraction method for identifying gait asymmetry using wearable sensors," *Sensors*, vol. 18, no. 2, Feb. 2018, Art. no. 676.
- [56] A. Dubois et al., "Automating the timed up and go test using a depth camera," *Sensors*, vol. 18, no. 1, Dec. 2017, Art. no. 14.
- [57] J. Beyea et al., "Convergent validity of a wearable sensor system for measuring sub-task performance during the timed up-and-go test," *Sensors*, vol. 17, no. 4, Apr. 2017, Art. no. 934.
- [58] S. Fudickar et al., "Measurement system for unsupervised standardized assessment of timed 'up & go' and five times sit to stand test in the community—A validity study," *Sensors*, vol. 20, no. 10, 2020, Art. no. 2824.
- [59] R. Morris et al., "Validity of MobilityLab (version 2) for gait assessment in young adults, older adults and Parkinson's disease," *Physiol. Meas.*, vol. 40, no. 9, Apr. 2021, Art. no. 095003.